Hyaluronan content governs tissue stiffness in pancreatic islet inflammation

Received for publication, September 27, 2017, and in revised form, November 10, 2017 Published, Papers in Press, November 28, 2017, DOI 10.1074/jbc.RA117.000148

Nadine Nagy[‡1], Adi de la Zerda[§], Gernot Kaber[‡], Pamela Y. Johnson[¶], Kenneth H. Hu[‖], Michael J. Kratochvil[‡§], Koshika Yadava[‡], Wenting Zhao[§], Yi Cui[§], Guadalupe Navarro[**], Justin P. Annes[**], Thomas N. Wight[¶], Sarah C. Heilshorn[§], Paul L. Bollyky[‡2], and Manish J. Butte[‡‡2,3]

From the [‡]Department of Medicine, Division of Infectious Diseases, the [§]Department of Materials Science and Engineering, [‖]Stanford Biophysics, the [**]Department of Medicine, Division of Endocrinology, and the [‡‡]Department of Pediatrics, Division of Immunology, Allergy, and Rheumatology, Stanford University, Stanford, California 94305 and the [¶]Matrix Biology Program, Benaroya Research Institute, Seattle, Washington 98101

Edited by Amanda J. Fosang

We have identified a novel role for hyaluronan (HA), an extracellular matrix polymer, in governing the mechanical properties of inflamed tissues. We recently reported that insulitis in type 1 diabetes of mice and humans is preceded by intraislet accumulation of HA, a highly hygroscopic polymer. Using the double transgenic DO11.10 × RIPmOVA (DORmO) mouse model of type 1 diabetes, we asked whether autoimmune insulitis was associated with changes in the stiffness of islets. To measure islet stiffness, we used atomic force microscopy (AFM) and developed a novel "bed of nails"-like approach that uses quartz glass nanopillars to anchor islets, solving a long-standing problem of keeping tissue-scale objects immobilized while performing AFM. We measured stiffness via AFM nanoindentation with a spherical indenter and found that insulitis made islets mechanically soft compared with controls. Conversely, treatment with 4-methylumbelliferone, a small-molecule inhibitor of HA synthesis, reduced HA accumulation, diminished swelling, and restored basal tissue stiffness. These results indicate that HA content governs the mechanical properties of islets. In hydrogels with variable HA content, we confirmed that increased HA leads to mechanically softer hydrogels, consistent with our model. In light of recent reports that the insulin production of islets is mechanosensitive, these findings open up an exciting new avenue of research into the fundamental mechanisms by which inflammation impacts local cellular responses.

It was recently reported that pancreatic β-cells are mechanosensitive, *i.e.* that their viability and function are impacted by their local mechanical environment. In particular, clusters of β-cells derived from mice or from the Min6 β-cell line increase insulin transcription when grown on soft *versus* stiff substrate (1). However, the relevance of this finding to autoimmune insulitis was unclear because tissue stiffness had not been known to change in the setting of inflammation.

The mechanical properties of tissues are influenced by the constituent cells and extracellular matrix (ECM),[4] as well as their interactions. These include polymer-tangling interactions or cross-linking, both of which are dynamic and are influenced by the molecular mass of the polymers. Viscoelasticity of the matrix is further influenced by the time-dependent movement of matrix fibers and by the movement of water and other solutes. The cells embedded in the matrix add an important influence because of their adhesion (anchoring) and traction on the matrix. However, the mechanical and matrix properties of tissues during inflammation and autoimmunity have not previously been considered, to our knowledge. Moreover, the factors that govern tissue mechanics in the setting of active inflammation and edema are not well-understood.

One factor that we suspected might play a role in tissue mechanics during inflammation is hyaluronan (HA), an ECM glycosaminoglycan that is abundant at sites of both acute and chronic inflammation in a variety of tissues (2, 3). HA is synthesized by three hyaluronan synthase (HAS) enzymes (4). HA levels are greatly elevated in injured tissues, with production increasing by as much as 80-fold over baseline (5, 6). Because HA is highly hygroscopic, this increased HA production seems

This work was supported by Deutsche Forschungsgemeinschaft Grants NA 965/2-1 (to N. N.) and KA 3441/1-1 (to G. K.); National Institutes of Health Grants R01 DK096087-01, R01 GM111808, and U01 AI101984 (to P. L. B.), R01 DK101530 (to J. P. A.), and R01 GM110482 (to M. J. B.); National Institutes of Health Pilot Project Grant U01 AI101990 (to T. N. W.); a National Science Foundation Graduate Research Fellowship (to A.d. l. Z.); National Science Foundation Grant CBET-1264833 (to M. J. B.); a P&F award from the Stanford Diabetes Research Center (to N. N.); a grant from the Stanford ChEM-H Interdisciplinary Postdoctoral Training Program in Quantitative Mechanobiology (to M. J. K.); Juvenile Diabetes Research Foundation Grants 1-SRA-2018-518-S-B (to P.L.B.), nPOD 25-2010-648 (to T. N. W.), and 3-PDF-2014-224-A-N (to N. N.); a Harrington Foundation grant (to P. L. B.); and a grant from the Stanford Child Health Research Institute (to M. J. B.). The authors declare that they have no conflicts of interest with the contents of this article. The content is solely the responsibility of the authors and does not necessarily represent the official views of the National Institutes of Health.

This article contains Figs. S1–S4.

[1] To whom correspondence should be addressed: Dept. of Medicine, Division of Infectious Diseases, Stanford University, 279 Campus Dr., Beckman Center, Rm. B237, Stanford, CA 94305-2805. Tel.: 650-723-8158; E-mail: nnagy@stanford.edu.

[2] These authors contributed equally to this work.

[3] Present address: Dept. of Pediatrics, Division of Immunology, Allergy, and Rheumatology, University of California Los Angeles, Los Angeles, CA 90095.

[4] The abbreviations used are: ECM, extracellular matrix; HA, hyaluronan; T1D, type 1 diabetes; AFM, atomic force microscopy; 4-MU, 4-methylumbelliferone; HAS, hyaluronan synthase; HMM, high molecular mass; LMM, low molecular mass; hyal, hyaluronidase; IHC, immunohistochemistry; CFSE, carboxyfluorescein succinimidyl.

© 2018 by The American Society for Biochemistry and Molecular Biology, Inc. Published in the U.S.A.

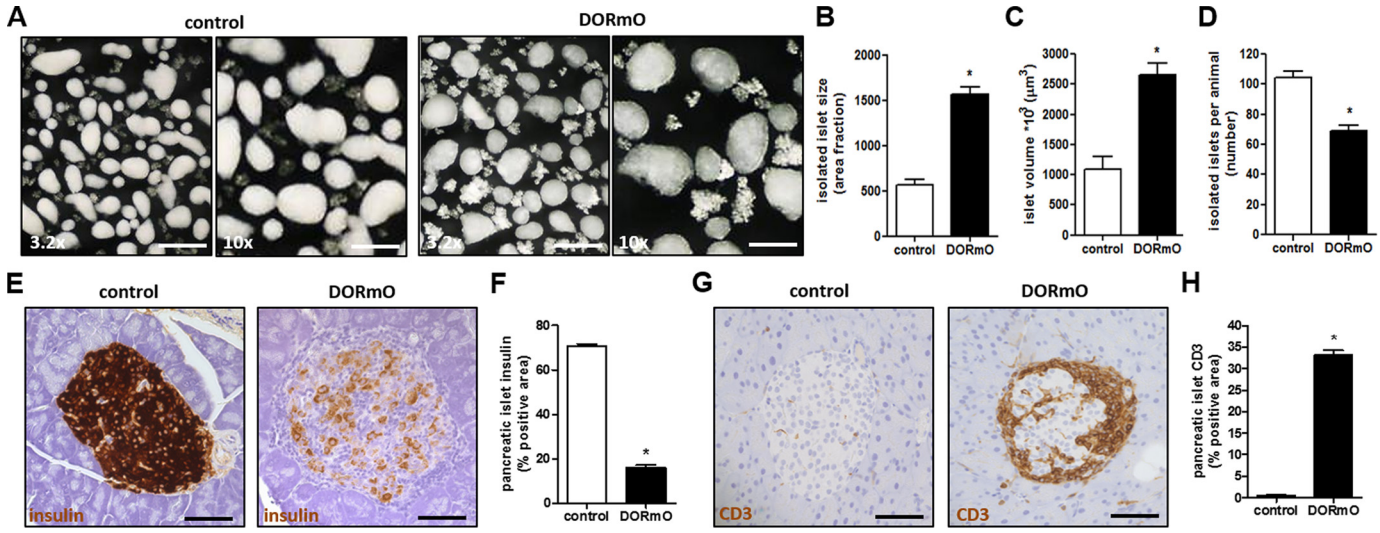

Figure 1. Autoimmune insulitis is associated with increased islet volume. *A*, representative dark-field images of isolated islets from 8-week-old control (Balb/c) and DORmO mice. The pictures were taken at a 3.2× (*left panels*) and 10× (*right panels*) magnification. *B* and *C*, islet size (*B*) and volume (*C*) were measured from 20 islets/animal ($n = 6$ mice/group). *D*, the number of islets isolated per animal, counted manually. *E* and *G*, representative histological staining of insulin (*E*) and CD3 (*G*) in pancreas tissue from control and DORmO mice, shown in brown. *F* and *H*, average islet area positive for insulin (*F*) and CD3 (*H*) staining, evaluated from histologic staining of pancreas tissue from control and DORmO mice. *Bars* show means ± S.E. *, $p < 0.05$ *versus* control by unpaired *t* test.

likely to drive edema at sites of injury. Indeed, HA has been implicated in vascular permeability changes (7–9), as well as leukocyte adhesion and egress (10, 11). Many chronic disease processes associated with unremitting inflammation are also associated with prolonged increases in HA, including type 2 diabetes (12), liver cirrhosis (13), and several autoimmune diseases (14, 15).

We chose to evaluate the role of HA in tissue mechanics in autoimmune insulitis, a well-characterized and medically relevant form of inflammation that precedes type 1 diabetes (T1D), in which HA is known to be a prominent feature of the disease (16). In this disease, the immune system attacks and destroys insulin-producing β-cells that reside within pancreatic islets, thereby leaving the affected individual perilously dependent on exogenous insulin for survival (17). Islets themselves are ovoid structures of endocrine tissues that are embedded within the larger, exocrine pancreas. Because islets are well-defined and structurally cohesive units that harbor localized, self-contained inflammation in the setting of autoimmunity, they are well-suited for mechanical analysis. Recently, we reported that autoimmune insulitis was associated with islet-specific deposition of HA in both human T1D (16), as well as in animal models of the disease, including non-obese diabetic mice (18) and DO11.10 × RIPmOVA (DORmO) mice (19).

In this study we establish the relationship between insulitis-induced depositions of HA in islets and the change in islet stiffness. We measured islet stiffness using atomic force microscopy (AFM) of healthy and insulitis diseased islets. To do so we developed a novel approach for anchoring islets from diabetic and control mice for AFM using quartz glass nanopillars, solving a long-standing problem of keeping tissue-scale objects from moving while performing AFM (20, 21).

Additionally we tested the role of HA in islet stiffness using a specific inhibitor of HA synthesis, 4-methylumbelliferone (4-MU) (22, 23), which was added to the chow of prediabetic mice. We previously demonstrated that this treatment reduced HA levels in both the serum and islets of DORmO mice (19).

Together, these tools allowed us to interrogate the role of HA in tissue stiffness during autoimmune insulitis. In particular, we test the hypothesis that increases in HA content during inflammation promote the softening of inflamed tissues, whereas reductions in HA promote a return to basal levels of stiffness.

Results

Autoimmune insulitis is associated with increased islet volume

We first characterize the size of pancreatic islets during insulitis. To this end, we isolated islets of control Balb/c mice and prediabetic DORmO mice (Fig. 1*A*). When the islets were examined at a higher magnification, we observed a more irregular shape and an increase in the size of the DORmO islets (Fig. 1*A*). Analyzing that, we found a 3-fold increase in size (Fig. 1*B*) and a 2.5-fold increase in islet volume (Fig. 1*C*) of islets from prediabetic DORmO mice compared with controls. We also found that prediabetic DORmO mice at 8 weeks of age already had a significant decrease in the number of islets, compared with age-matched control mice (Fig. 1*D*). The functional pancreatic islet characteristics like insulin, produced by β-cells, and glucagon, produced by α-cells, were examined via immunohistochemistry. We saw a significant reduction of insulin-positive staining in the pancreatic islets of the DORmO mice compared with controls (Fig. 1, *E* and *F*), whereas the glucagon content in the DORmO mice was only slightly lowered compared with controls (Fig. S1, *A* and *B*).

Autoimmune insulitis is prominent in young DORmO mice

The increase in islet size and the loss of insulin-producing β-cells is consistent with the infiltrative nature of autoimmune insulitis. Many of the expected infiltrating cells are $CD45^+$ lymphocytes (24), including T cells (19) and macrophages. Infiltrating cells in and around the DORmO islets were found to express

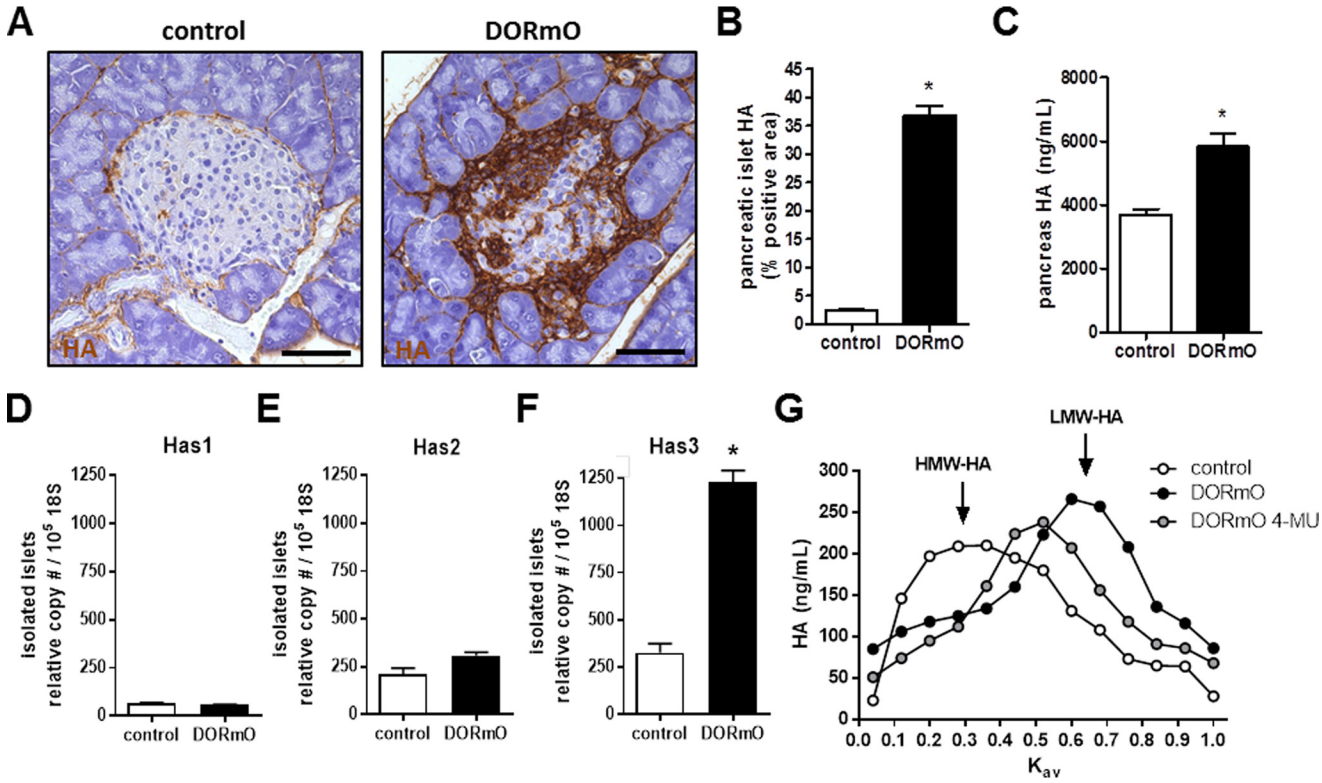

Figure 2. Autoimmune insulitis is associated with accumulation of HA. *A*, representative histologic staining of HA in pancreas tissue from control and DORmO mice, shown in *brown*. *B*, HA staining, evaluated from histologic staining of pancreas tissue from control and DORmO mice. *C*, pancreas HA content from control and DORmO mice. *D–F*, mRNA expression levels of HAS1 (*D*), HAS2 (*E*), and HAS3 (*F*) of isolated islets from control and DORmO mice. *G*, representative HA size column profile from pancreatic islets from control, DORmO, and 4-MU–fed DORmO mice ($n = 300$ islets/column run). *Bars* show means ± S.E. *, $p < 0.05$ *versus* control by unpaired *t* test.

CD3, which is the T cell co-receptor involved in the activation of cytotoxic T cells and T helper cells (Fig. 1*G*). Quantification of the CD3 staining demonstrates that DORmO mice have significantly more CD3-positive infiltrating cells compared with control mice (Fig. 1*H*). A CD3-positive staining in the control mice could only be detected at sites of vessels inside the islet (Fig. 1*G*). Furthermore, in the areas of infiltration, a significant increase of macrophages (Fig. S1, *C* and *D*) and apoptotic cells (Fig. S1, *E* and *F*) could be detected as shown by F4/80 and caspase 3-positive staining. The collective presence of these markers clearly shows the destructive nature of autoimmune insulitis in the DORmO mouse model. These findings implicate the presence of multicellular insulitis and demonstrate that insulitis was present at the time the islets were used in these experiments.

HA is abundant in autoimmune insulitis

Our prior work has shown that HA accumulates in human islets during disease (16), as well as in mouse models of T1D (Fig. 2*A*). We quantified the accumulation of HA in the DORmO T1D mouse model and found a >20-fold increase in 8-week-old prediabetic DORmO mice compared with controls (Fig. 2*B*). This result agrees with our findings in these mice at other time points. In control mice HA was only found in the adventitial tissue, around the islet capsule, and around vessels inside and outside the islet (Fig. 2*A*). In contrast, the distribution of HA in the DORmO mice was much more prominent at the sites of invading cells, at the islet borders, and around intraislet vessels (Fig. 2*A*). Consistent with the increased accumulation of HA around the islet area in the DORmO mice, a significant increase of HA was detected when the whole pancreas was measured and compared with control mice (Fig. 2*C*). Looking at transcripts of HASs from isolated islets, we found significant differences in HAS3 expression between islets of DORmO and control mice (Fig. 2*F*). In contrast, the expression of HAS1 was slightly down-regulated in the DORmO mice (Fig. 2*D*), and HAS2 was slightly up-regulated (Fig. 2*E*) compared with control mice. To better understand the accumulation of HA in islets, we examined the role of HA degradation by hyaluronidases (hyal) and found that HYAL1 was down-regulated in isolated islets of DORmO mice, whereas HYAL2 was up-regulated (Fig. S2, *A* and *B*). HYAL2 cleaves high molecular mass (HMM)-HA resulting in small HA fragments that are mainly found in inflammatory settings. The increases of HAS3 and HYAL2 found in the pancreatic islets agree with our DORmO mouse model of autoimmune insulitis where inflammation is prominent. Another route by which HA could be degraded is through the action of reactive oxygen species. To investigate whether treatment with 4-MU diminishes HA through this mechanism, we treated INS-1, a β-cell line, with 4-MU and measured intracellular reactive oxygen species. We did not detect an increase in cellular oxidative stress compared with untreated cells (Fig. S2*C*). These results show that HA accumulation and its associated inflammation in diabetes are due to a combination of increased synthesis and cleavage of HA but not reactive oxygen.

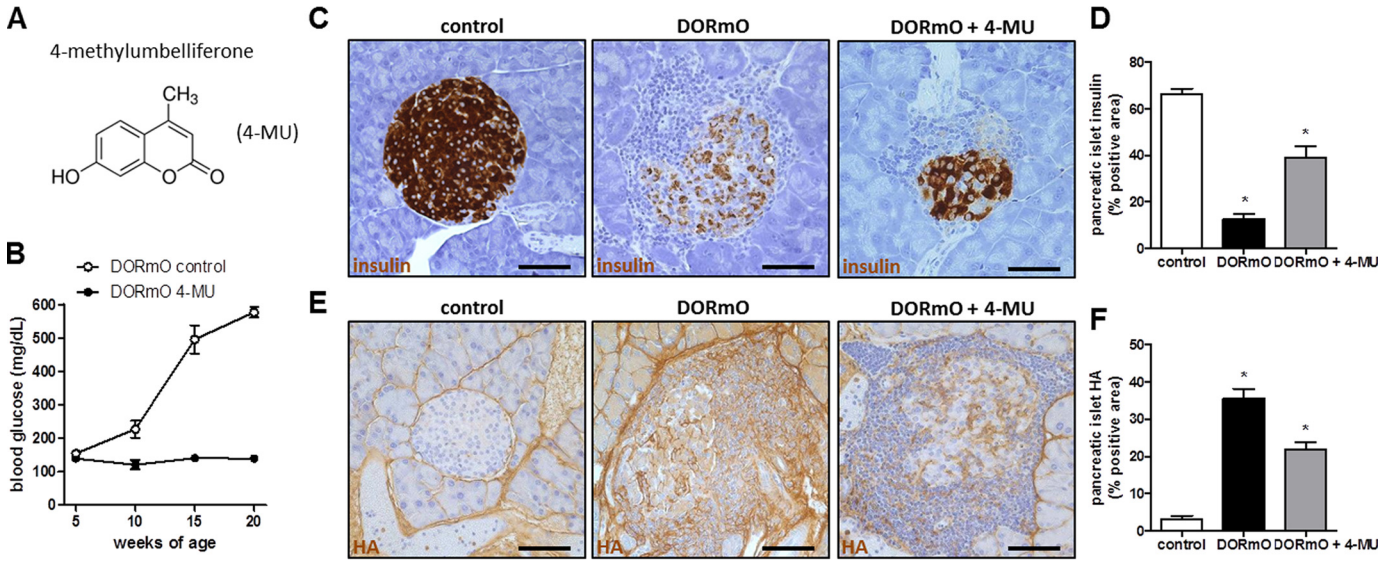

Figure 3. HA inhibition prevents mice from becoming hyperglycemic. *A*, molecular structure of 4-MU. *B*, blood glucose of DORmO mice fed 4-MU chow or control chow ($n = 10$ mice/group). *C* and *E*, representative insulin (*C*) and HA (*E*) staining of pancreatic tissue from control, DORmO, and 4-MU–fed DORmO mice. *D* and *F*, insulin (*D*) and HA (*F*) staining, evaluated from histologic staining of pancreas tissue from control, DORmO, and 4-MU–fed DORmO mice. *Bars* show mean ± S.E. *, $p < 0.05$ *versus* control by unpaired *t* test.

We also investigated CD44, the major cell surface receptor of HA. Similar to HA, CD44 accumulation and distribution could mainly be detected in mice with autoimmune insulitis (Fig. S1*G*). CD44-positive staining showed a 20-fold increase in the DORmO islets compared with control mice (Fig. S1*H*).

Autoimmune insulitis is associated with accumulation of low molecular mass (LMM)-HA fragments

Measuring the HA size in isolated pancreatic islets from control mice and treated and untreated DORmO mice via size exclusion column revealed three very different profiles. The peak of the curve for control mice was found at lower K_{av} compared with DORmO mice, meaning the HA found in the isolated control islets mainly consist of HMM-HA (Fig. 2*G*). The peak of the untreated DORmO curve on the other hand was at higher K_{av}, meaning that predominately LMM HA was found in those isolated islets (Fig. 2*G*). The peak and the whole curve of the 4-MU–treated DORmO mice lies in between the controls and untreated DORmO mice, meaning, that the 4-MU–treated DORmO mice islets shift from LMM-HA in the direction of HMM-HA (Fig. 2*G*). We also observed that the total amount of HA is lower in 4-MU–treated DORmO islets compared with untreated DORmO islets (Fig. 2*G*). Furthermore, we investigated the effect of HMM-HA and LMM-HA on T cells in high (4.5 g/liter) and low (2 g/liter) glucose conditions to reflect different diabetic conditions. HA sizes between 50 kDa and 1.8 MDa had no impact on T cell proliferation in the different glucose conditions (Fig. S3). Even a hyaluronidase digestion of 100 kDa did not show any effect on T cell proliferation (Fig. S3). Taken together, these results show that inflamed islets accumulate fragmented, inflammatory HA, whereas 4-MU treatment reduces this effect.

HA inhibition prevents mice from becoming hyperglycemic

Having established that HA is abundant at sites of autoimmune insulitis, we examined the effect of HA inhibition on insulitis progression in T1D. To achieve that, we used the small molecule inhibitor 4-MU (Fig. 3*A*), which was administered orally to the mice, at a dose shown to be effective before (19). 4-MU treatment beginning at 5 weeks of age appeared to stop the progression of diabetes as compared with untreated controls (Fig. 3*B*). Additionally 4-MU–treated DORmO mice had significant more insulin-positive areas (Fig. 3, *C* and *D*) and significantly fewer HA-positive areas (Fig. 3, *E* and *F*) in the pancreatic islets compared with untreated controls, as shown and quantified by immunohistochemistry.

Because 4-MU is primarily metabolized in the liver when administered orally, we investigated the influence of 4-MU on liver function. A liver panel with aspartate aminotransferase, alanine aminotransferase, alkaline phosphatase, γ-glutamyl transferase, and total and direct bilirubin was measured in the serum from control and prediabetic DORmO mice with and without 4-MU treatment (Fig. S4). All markers showed no difference between the treatment groups. Alkaline phosphatase and γ-glutamyl transferase were not detected in either group (data not shown). Aminotransferase was a little higher in the control animals compared with DORmO mice, but there was no difference caused by 4-MU treatment in either mouse group (Fig. S4). Total and direct bilirubin were slightly elevated in the 4-MU treatment groups, but the difference was not significant (Fig. S4). These results indicate that 4-MU does not cause hepatocyte toxicity or cholestasis.

Nanopillar preparation of islet AFM samples

To study whether the changes in morphology and chemical composition resulted in a mechanical change in the islets, we examined the elastic modulus of islets by AFM. It has been a long-standing problem to anchor and measure soft tissue samples, particularly in the size regime of islets. Epoxies can permeate the tissue samples and artificially increase the measured stiffness (21). Clamps or plates can result in squeezing fluids from one part of the tissue into another. These effects could

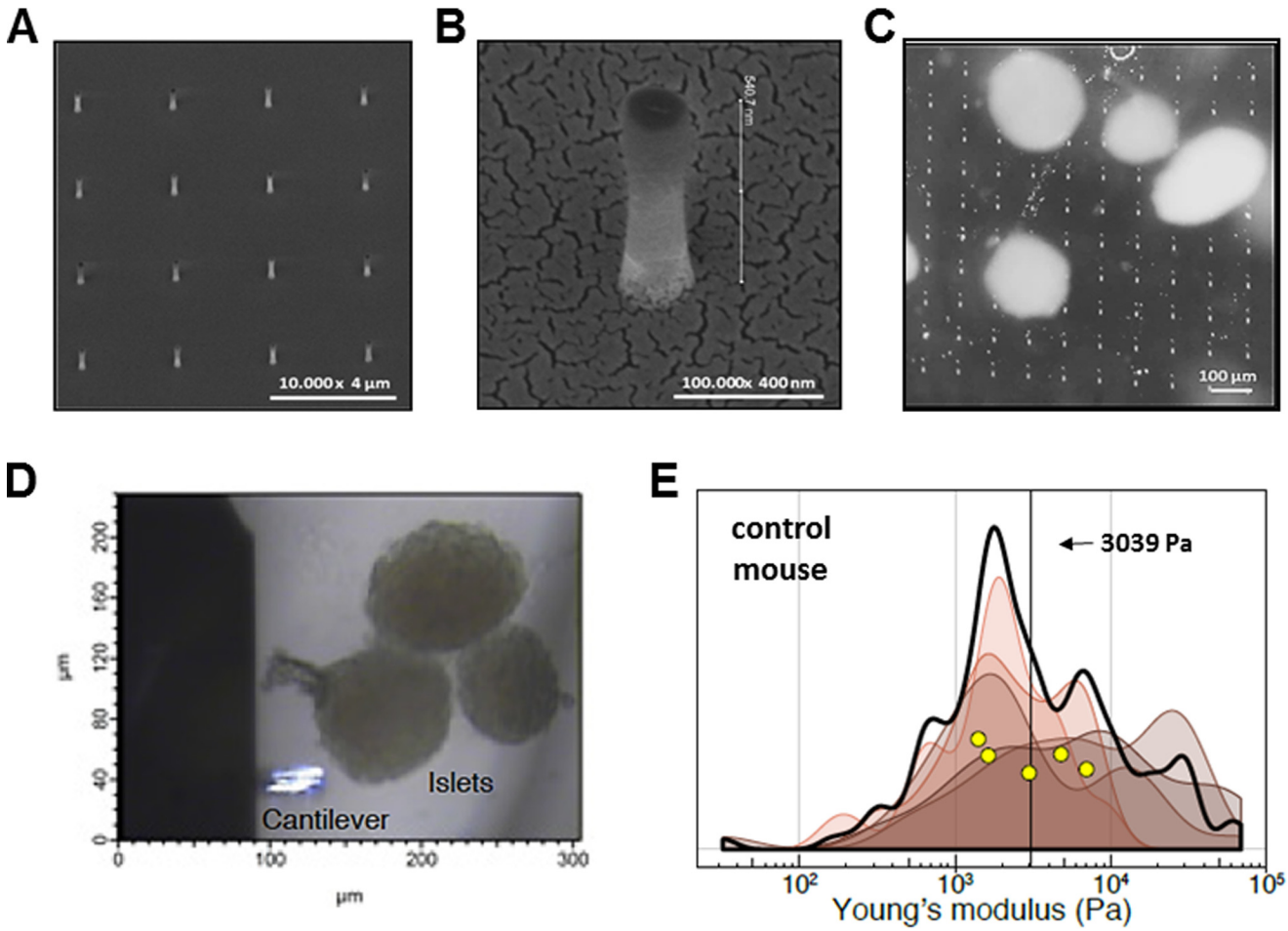

Figure 4. Islets measured by AFM were anchored by impaling them. *A* and *B*, representative electron microscopy of glass cylindrical nanopillars. The nanopillars arose from a glass base and were measured to be ~1000 nm tall, 200 nm in diameter, and spaced by 3 μm center to center. *C*, freshly isolated islets from mice were transferred onto the nanopillars. The individual nanopillars were not visible here, but 5-μm-square fiducials placed periodically with the array of pillars are seen. *D*, bright-field images of AFM cantilever (*lower left*) and three islets anchored on the nanopillar array (not visible in this focal plane) to be scanned. *E*, five independent islets from control mice were measured on average 28 discrete points each. Elastic moduli calculated from these indentations are graphed as a smoothed histogram; each *shade* represents a different islet. The *black curve* indicates the sum distribution. *Yellow circles* are the mean stiffness for each islet. The *vertical black line* at 3039 Pa is the average.

especially distort the measured elasticity of tissues rich with HA.

We developed an innovative approach for anchoring islets that involves attaching them upon nanopillars. Sharp nanopillar-decorated surfaces similar to the ones used in this study have been previously shown to impair cell movement at the single cell level (25). If the impalement is relative shallow compared with the size of the tissue, it will prevent sample movement while leaving the upper surface of the tissue mechanically unaltered for measurement by AFM. We prepared an array of cylindrical nanopillars on quartz glass using electron beam lithography and deep reactive-ion etching (Fig. 4*A*) (26). The nanopillars arose from a glass base and were characterized by scanning electron microscopy (Fig. 4*B*). We attached the glass base of the nanopillars onto the bottom of a Petri dish by double-sided tape before carefully placing islets onto the pillars. Gentle centrifugation of the islets on the pillars was used to fix samples in place without damaging the samples (see "Experimental procedures") (Fig. 4*C*). The islets were then transfixed and did not move with tilting of the Petri dish.

HA leads to mechanically soft islet tissue

We performed AFM on islets obtained from healthy control mice (Fig. 4*D*). We chose a spherical colloidal probe to reduce the chance of piercing the soft islet matrix and to perform spatial averaging. Based on visual examination, indentation measurements were chosen to occur in the flat, "top" region of each islet, thus minimizing chances of a collision between the cantilever base and the islet. Force-distance map measurements were performed, and each control mouse islet was measured a median of ~32 times (n = 5 islets). Elastic moduli calculated from each islet were graphed as smoothed histograms (Fig. 4*E*). The elasticity of each islet measured spanned a range from 100 Pa to 10 kPa, with an average of 3,039 Pa (Fig. 4*E*, *vertical black line*). These results indicate that the mechanical stiffness of healthy islets is ~3 kPa.

4-MU treatment makes inflamed islets stiffer

We next performed AFM on islets isolated from prediabetic DORmO mice that had been fed with control chow or 4-MU chow (Fig. 5*A*) for at least 2 weeks. Force-distance map mea-

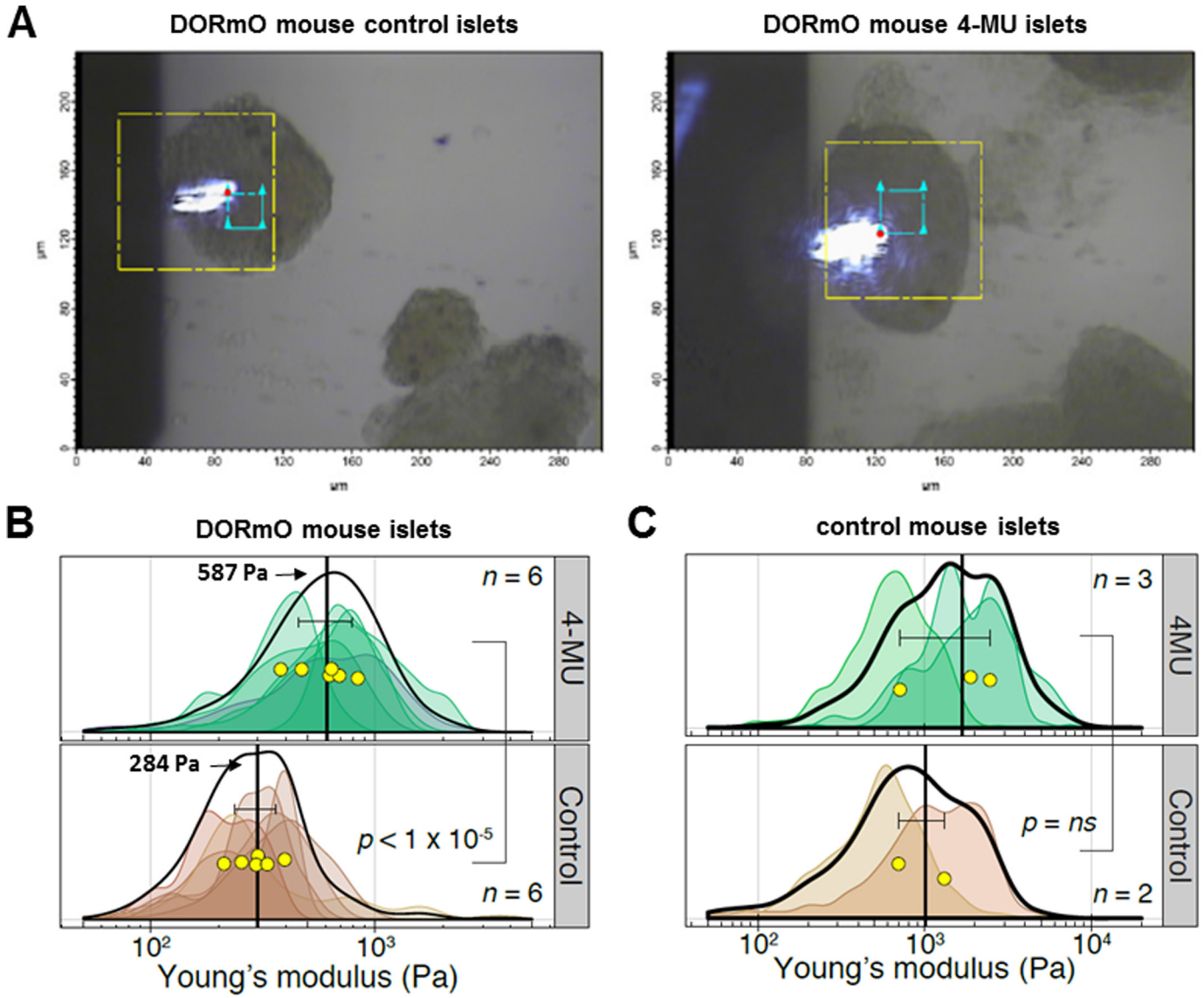

Figure 5. Islets of prediabetic DORmO mice measured by AFM. *A*, bright-field images of AFM cantilever scanning an islet isolated from a DORmO prediabetic mouse fed with control chow or 4-MU chow. The *yellow box* represents the scan area of the AFM stage (~90 μm × ~90 μm), whereas the *blue box* shows a typical area scanned for each islet (20-μm box). *B*, islets from DORmO mice fed 4-MU chow or control chow. Six independent islets for each treatment group were measured on average 166 discrete points each. Elastic moduli calculated from these indentations are graphed as a smoothed histogram; each *shade* represents a different islet. The *black curve* indicates the sum distribution. *Yellow circles* are the mean stiffness for each islet. The *vertical black lines* are the average stiffnesses for each group, with *error bars* showing the 95% confidence interval. *C*, islets from control (Balb/c) mice fed 4-MU chow or control chow. Elastic moduli for points of each islet shown as smoothed histograms; each *shade* represents a different islet. The *black curve* indicates the sum distribution. *Yellow circles* are the mean stiffness for each islet. The *vertical black lines* are the average stiffnesses for each group, with *error bars* showing the 95% confidence interval.

surements were performed, and each islet was measured an average of ~166 times each (n = 6 islets in each group). We found the islets from prediabetic DORmO mice had a mean elastic modulus of 284 Pa (Fig. 5*B*, *vertical bar*). Thus, the accumulation of HA in these prediabetic islets led to a significant decrease of mechanical stiffness compared with healthy mice. On the other hand, 4-MU–treated DORmO mice had a mean modulus of ~587 Pa (Fig. 5*B*) approximately twice as stiff as the non-treated DORmO mice islets. In a second independent experiment (n = 9 control chow, n = 11 4-MU chow), the islets from 4-MU–fed DORmO mice were again statistically significantly stiffer than those from DORmO mice fed control chow (p = 0.01). Thus, reducing accumulation of HA with 4-MU results in partial restoration of mechanical stiffness. These findings show that accumulation of HA in the islets results in mechanical softening of the tissues and that treatment with an inhibitor of HA synthesis partially rescues the tissue mechanical properties to that of healthy, non-insulitis islets.

We then examined the effects of 4-MU on the stiffness of islets isolated from control animals without insulitis. Stiffness of islets from control Balb/c mice did not change significantly after feeding 4-MU chow (Fig. 5*C*). These results indicate that 4-MU does not alter the mechanical properties of islets in the absence of inflammation. In light of our previous report that healthy islets contain only minimal HA (19), these data are consistent with the model that 4-MU-mediated effects on islet stiffness are mediated through effects on HA.

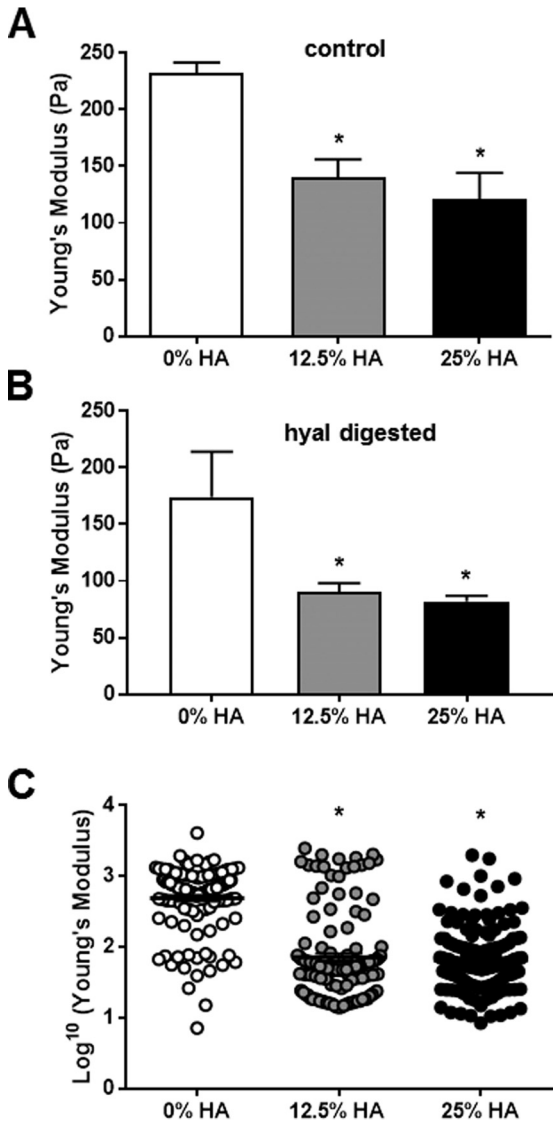

Figure 6. Increased HA content leads to mechanically soft hydrogels. *A*, stiffness measurements via rheometer of cross-linked hydrogels with 0–25% total HA content. *B*, stiffness measurement via rheometer of hyal-treated cross-linked hydrogels with 0–25% total HA content. *C*, stiffness measurement via AFM of cross-linked hydrogels with 0–25% total HA content. Stiffness is expressed as Young's modulus in Pa. The data show means ± S.E. *, $p < 0.05$ *versus* control by unpaired *t* test.

Increased HA content leads to mechanically softer hydrogel tissue models

Having established that the increase of water is associated with higher HA content in islets, we now wanted to investigate the role of hyaluronan concentration in altering the mechanical properties of hydrogels that model the mechanical behavior of tissues. We examined Matrigel mixed with different concentrations of 100-kDa HA. The final concentration of HA in the hydrogels were 25, 12.5, and 0% (by weight), respectively, with a constant concentration of Matrigel in each and total volume. Using shear rheology, we found that all HA-containing gels were softer than unmodified Matrigel (Fig. 6*A*). The highest HA-concentration gel showed a decrease of ~45% in the Young's modulus (~110 Pa) compared with the unmodified Matrigel (Fig. 6*A*).

In a separate experiment we added hyal-digested HA at the same concentrations as used before. We found that the hyal-treated HA hydrogels were even softer than the untreated HA hydrogels independent of the containing HA concentration (Fig. 6*B*), suggesting that reduced polymer size contributes to softening of hydrogels.

In a second model system, we used a thiolated collagen-based hydrogel system covalently cross-linked with PEG-based linker. Similar to before, this system was doped with various amounts of HA while maintaining the same concentration of the collagen component and cross-linker density. The stiffness properties of these materials were measured in PBS buffer with AFM, the same technique used for measuring islet stiffnesses. Using AFM with the HA hydrogels, we observed similar trends, with increasing HA concentration resulting in softer hydrogels (Fig. 6*C*).

Discussion

We report here that inflamed islets are softer than healthy islets and that increases in local content of HA are a major driver of tissue stiffness. This paper is the first study to our knowledge to 1) examine the tissue mechanics of islets, 2) quantify effects of inflammation on local tissue mechanics, and 3) implicate HA in tissue biomechanics. Given the recent report that primary β-cells are mechanosensitive and alter their insulin production in response to tissue stiffness (1), these findings here may provide a critical link between inflammation and β-cell dysfunction in T1D.

Along with decreasing stiffness in inflamed islets, we find that increased HA content and reduced HA size both lead to a decrease in hydrogel stiffness. This is consistent with previous reports showing that increased HA concentration within HA collagen hydrogels significantly decreased shear storage modulus and increased compressive resistance (34). Those authors reported that HA-induced effects on viscoelastic properties result primarily from modulation of the interstitial fluid. Other studies suggest that HA influences islet cell biology in multiple ways, including effects on insulin release and viability (28–32).

Our model is that increased HA content reduces tissue stiffness through effects on the organization of water. It is well-established that networks of charged glycosaminoglycan polymers, like HA, trap water and restrict its movement. For this reason, HA is a common component of hydrogels (27). Further, the content of HA within a hydrogel is known to be related to its viscosity (33, 34) and stiffness (27, 35). Similarly, increased HA content within tissues is known to cause them to swell, resulting in edema (36). We propose that the hydroscopic properties of HA may recruit and order water molecules within tissues and hydrogels, thus acting as a cushioning and lowering the stiffness properties in these cases. LMM-HA may enhance this softening because the movement and fluidity of shorter HA polymers can be expected to be more fluid. HA and LMM-HA in particular may thereby be a major contributor to the mechanical properties of inflamed tissues, including islets under autoimmune attack.

Inflamed islets are mechanically soft, and this may be relevant to the pathophysiology of autoimmune insulitis. It was recently reported that stiffness modulates T lymphocyte migra-

tion and morphological changes induced by TCR/CD3 triggering (44). Softer materials were recently reported to increase insulin mRNA expression of 3D primary mouse islet-derived and Min6-derived β-cell clusters (45).

It is well-known that physiological processes within inflamed tissues are affected by the stiffness of the ECM, which can affect many of the biological activities of the cells living within. For example, stem cells alter their differentiation and even their capacity for self-renewal and differentiation based on the elasticity of the tissue (37, 38). Cancer cells alter their proliferation and metastatic potential based on the mechanical properties of the matrix (39, 40). We recently showed that the speed of migrating T cells, like many circulating immune cells, is influenced by the presence of HA (41). Other factors include the porosity and mechanics of the tissue (42). We are currently working to understand how tissue stiffness impacts the production and secretion of insulin and other endocrine hormones produced by islets. Of note, we recently reported that 4-MU did not affect serum insulin levels in Balb/C mice (17). Thus, the rescue of insulin production in the islets by 4-MU is specific to diabetes.

Reducing the accumulation of HA in T1D using the small-molecule inhibitor 4-MU results in a return to basal levels of mechanical stiffness. Having previously reported that this same treatment promotes the resolution of autoimmunity (19), we suggest that HA and mechanically soft islets may play a fundamental mechanism in engendering autoimmunity. 4-MU reduces accumulation of HA in other autoimmune diseases such as experimental autoimmune encephalomyelitis (41, 43), the mouse model of multiple sclerosis, and it is tempting to speculate that T cell responses in T1D (19) and experimental autoimmune encephalomyelitis are reduced because of 4-MU– and HA-mediated effects on tissue mechanics. However, HA inhibition and 4-MU have other effects in addition to fluid shifts (reviewed in Ref. 23), and the relative importance of these to immune activation has not yet been elucidated. Also, 4-MU may have spasmolytic and choleretic activities that are not linked to the activities of HA synthases. The importance of tissue mechanics in cellular differentiation and cancer metastasis has been well-established, but this work is the first to posit a role in autoimmunity.

The development of nanopillars to anchor islets in place is an innovative solution to the challenge of performing AFM on these tissues. We chose a large colloidal indenter and utilized modest indentations to reduce the influence of the structures situated beneath the ECM. However, the AFM measurements here entailed *in situ* measurements of the islet ECM but may amalgamate the mechanical influence of underlying cells or other structures.

This study has a few limitations. First, we have not investigated the contributions of HA-binding proteins (hyaladherins) to HA-mediated effects on tissue stiffness. Hyaladherins, including TSG-6 (TNF-stimulated gene-6), and inter-α-inhibitor, play critical roles in determining the longevity, size, and architecture of HA in tissues (44). These molecules could therefore be expected to influence tissue stiffness along with HA (45). Indeed, the catabolism of HA plays an important role in tissue homeostasis *versus* inflammation because HMM-HA and LMM-HA activate different receptors (46). Indeed, high-molecular-weight HA is anti-inflammatory and promotes resolution of local immune responses (46). Here we show that 4-MU alters this balance, shifting the LMM-HA in the direction of HMM-HA.

Moreover, many other cellular (47) and ECM components (16, 19, 48) of pancreatic islets might further impact the mechanical properties of islets during both health and disease. Along with water movement, increased cellularity caused by the abundance of activated $CD4^+CD44^+$ T cells may also contribute to the mechanical changes. Matrix components, such as glycated proteins and glycosaminoglycans, are ionically charged and can electrostatically trap the diffusion cytokines and molecules in the matrix (49–51).

In conclusion, islets of autoimmune diabetes are mechanically soft because of accumulation of HA. Understanding what regulates changes in the matrix components may be of critical importance to appreciate why tissue-specific autoimmune diseases arise in the first place. Thus, understanding whether tissue factors such as matrix stiffness promote ongoing autoimmunity opens the opportunity to intervene and prevent autoimmunity, perhaps with small-molecule inhibitors like 4-MU. This new perspective opens the possibility of developing other treatments that target the mechanical properties of tissues in T cell–mediated diseases.

Experimental procedures

Mice

All animals were bred and maintained under specific pathogen-free conditions, with free access to food and water, in the vivarium at the Benaroya Research Institute or in the animal facilities at Stanford University. Balb/c and DO11.10 transgenic mice were purchased from The Jackson Laboratory and bred with Balb/c mice expressing RIPmOVA (made available from the Benaroya Research Institute) to generate the DORmO double-transgenic mice.

4-MU treatment

4-MU (Alfa Aesar) was pressed into the mouse chow by TestDiet® and irradiated before shipment, as previously described (10). We previously determined that this chow formulation delivers 250 mg/mouse/day, yielding a plasma drug concentration of 640.3 $\pm$ 17.2 nmol/liter in mice, as measured by HPLC-MS. Mice were initiated on the 4-MU chow at 6 weeks of age and were maintained on this diet until they were euthanized, unless otherwise noted.

Weight and diabetes monitoring

Beginning at 4 weeks of age, mice were weighed weekly as well as bled via the tail tip for the determination of their blood glucose level using a Contour blood glucose meter and blood glucose monitoring strips (Bayer Healthcare). When two consecutive blood glucose readings of 250 mg/dl or greater were recorded, the mice were considered diabetic. When two consecutive blood glucose readings of 300 mg/dl or greater were recorded, mice were euthanized.

Serum measurements

Mouse serum was obtained from 15-week-old mice if not indicated otherwise. Serum samples for the liver panel were measured by the Animal Diagnostic Laboratory at the Stanford School of Medicine. Analyses for the mouse liver panel were performed on a Dimension Xpand (Siemens) analyzer.

Islet isolation

Islets were isolated as described (52). Briefly, mice 8 weeks of age were anesthetized with 2,2,2-tribromoethanol in PBS. The bile duct was clamped at its distal (intestinal) end, and a 30-gauge needle was used to inflate each pancreas through the common bile duct with 4 ml of islet medium comprising RPMI 1640 containing 1.0 g of $NaHCO_3$, 10% FBS (S12450H; Atlanta Biologicals), 1 mM sodium pyruvate, and penicillin/streptomycin at 4 °C. The islet medium was supplemented with 0.8 mg/ml of collagenase P (11-249-002-001; Roche) and filtered (0.22-μm filter) prior to injection. Subsequently, two or three excised pancreata were placed in separate 50-ml conical centrifuge tubes and incubated in 5 ml of islet medium for 13 min at 37 °C. The medium was then decanted, fresh 4 °C islet medium was added, and the tubes were shaken vigorously to disrupt the pancreata. The tissue suspensions were filtered through a 30-mesh metal screen to remove large debris, the filtrates were pelleted by centrifugation, and the pellets were resuspended in 4 °C islet medium. The material was centrifuged through Histopaque 1077 to isolate the islets, which were washed and hand-picked before being resuspended in islet medium and maintained in a tissue culture incubator.

Tissue processing and imaging

Tissues for histochemistry were taken out of the animals and immediately transferred into 10% neutral buffered formalin or methyl Carnoy's solution. The tissue was processed to paraffin (ASP300 tissue processor; Leica Biosystems), and 5-μm-thick sections were cut (RM 2255 Microtome; Leica Biosystems).

All staining steps were performed on a Leica Bond Max™ automated immunohistochemistry (IHC) stainer (Leica Biosystems). For HA affinity histochemistry, the bond intense R detection kit (Leica Biosystems), a streptavidin-HRP system, was used with 4 μg/ml biotinylated HA-binding protein in 0.1% BSA-PBS as the primary. The bond polymer detection kit was used for all other IHC. This detection kit contains a goat anti-rabbit conjugated to polymeric HRP and a rabbit anti-mouse post-primary reagent for use with mouse primaries.

CD44 and insulin IHC required pretreatment using heat-mediated antigen retrieval with EDTA at high pH (bond epitope retrieval solution 2) for 10 min. CD44 IHC, sections were incubated 30 min with 0.5 μg/ml rat anti-CD44 (clone IM7; Thermo Scientific). Incubation with rabbit anti-rat IgG (Vector Labs), post-primary was added in lieu of the post-primary reagent from the kit. An incubation with rabbit anti-goat IgG (Vector Labs), post-primary was added in lieu of the post-primary reagent from the bond polymer detection kit. Cleaved Caspase 3 IHC was performed using 1:500 dilution of antibody (catalog no. 9661; Cell Signaling) after antigen retrieval as above. F4/80 IHC used monoclonal antibody clone A3-2 (catalog no. ab6640; Abcam) at a dilution of 1:125 without antigen retrieval. Insulin and glucagon monoclonal antibodies (catalog nos. I2018 and G2654; Sigma) were both diluted 1:1000 without antigen retrieval. CD3 IHC required pretreatment using heat-mediated antigen retrieval with high pH EDTA for 20 min. Subsequently sections were incubated with 2.5 μg/ml rabbit anti-CD3 (A0452; Dako), detection was performed using a bond polymer refine detection kit.

IHC images were visualized using a Leica DMIRB inverted fluorescence microscope equipped with a Pursuit 4-megapixel cooled color/monochrome charge-coupled device camera (Diagnostic Instruments). Images were acquired using the Spot Pursuit camera and Spot advanced software (SPOT Imaging Solutions; Diagnostic Instruments). Image analysis was performed accordingly using ImageJ (National Institutes of Health), as described previously (52).

HA size column and ELISA

Tissues were first lyophilized and weighed and then were digested with proteinase K (250 μg/ml) in 100 mM ammonium acetate, pH 7.0, overnight at 60 °C. After digestion, the enzyme was inactivated by heating to 100 °C for 20 min.

DEAE-Sephacel resins were equilibrated with 8 M urea buffer. The column was packed using a 300-μl matrix bed, by adding 600 μl of DEAE Sephacel slurry to an Econo column. Samples were loaded onto the columns, once the samples moved in the column was washed with 10 ml of 8 M urea buffer. HA was eluted using 300 μl of urea buffer with 0.25 M NaCl. Eluents were stored at −20 °C.

Fraction collector was set to collect fractions every 1.5 min, with a fraction volume of 0.3 ml. 200 μl of eluent containing 6–7 μg of HA of DEAE purified samples was loaded onto the analytic Sephacryl S-1000 column. Add 10 μl of vitamin B_{12} to mark the end of the column. Run HA standards to calibrate the column and elute with PBS at a slow rate of 12–15 ml/h.

Each fraction was measured in the HA ELISA to generate a HA profile. The total amount of HA was determined by a modified competitive ELISA in which the samples to be assayed were first mixed with biotinylated HA-binding protein and then added to HA-coated microtiter plates, the final signal being inversely proportional to the level of hyaluronan added to the biotinylated proteoglycan (53).

Quantitative PCR

Islets were harvested for total RNA isolation using the High Pure RNA isolation kit (Roche Applied Science) and reverse-transcribed using the high capacity cDNA reverse transcription kit (Applied Biosystems). For quantitative PCR, all reagents were supplied by Applied Biosystems, unless otherwise noted. Relative quantification of HAS1, HAS2, HAS3, HYAL1, and HYAL2 gene expression was performed using TaqMan gene expression assays: HAS1, Mm00468496_m1; HAS2, Mm00515089_m1; HAS3, Mm00515092_m1 HYAL1, Mm00476206_m1; and HYAL2, Mm01230689_g1, respectively. Briefly, 100 ng of cDNA was amplified in 1× TaqMan gene expression master mix with a 250 nM TaqMan probe in a 20-μl reaction. Data for mRNA expression are provided as means ± S.E. of the estimated copy number, normalized to 18S rRNA, and differences between enriched primary islet cell populations were analyzed.

Oxidative stress detection

INS-1 cells, a β-cell line, were treated with and without 300 μM 4-MU for 24 h. At the end of treatment, a CellROX® reagent (Thermo Fisher) was added for measuring cellular oxidative stress. Using flow cytometry, the MFI for the oxidative stress marker in the different treatment groups was calculated.

T cell proliferation

CD4+ T cells were positively selected from spleens and lymph nodes of naïve 10-bit C57Bl6 mice using MACS kits and labeled with carboxyfluorescein succinimidyl (CFSE) (Thermo Fisher) as per manufacturer recommendation. CFSE-labeled CD4+ T cells were stimulated for 72 h with 2 μg/ml of concanavalin A in the presence of T cell depleted, irradiated APCs in 96-well round bottom plates. HA (Lifecore) of indicated sizes was added to the culture at 20 μg/ml final concentration. At the end of 72 h, proliferation was measured by the dilution of CFSE-labeled CD4+ T cells on an LSR II flow cytometer. Proliferation index was calculated using FlowJo (Treestar version 9).

Atomic force microscopy

Islets were taken from prediabetic DORmO mice or control (Balb/c) mice treated with 4-MU or control chow for at least 2 weeks. The islets were fixed using 4% PFA for 15 min at room temperature and washed three times with PBS. AFM measurements required the islets to be stable and not moving while measuring. To anchor islets, we used a nanopillar array. The substrates consist of a regular array of vertical quartz nanopillars, fabricated on quartz coverslips (26) and taped to the bottom of a Fluorodish Petri dish (World Precision Instruments). The diameter of each pillar was ~200 nm, whereas the length of each pillar was ~1 μm, and the distance between pillars was 3 μm. Because the nanopillars are small, they are not visible through a low magnification objective (*e.g.* 20×). To facilitate localization of the pillars, we fabricated a 5-μm × 5-μm square for each set of 33 × 33 nanopillars (Fig. 4*C*). We placed ~5 μl of fixed islets in PBS onto the center of the nanopillar array, which was spun down (100 rpm, 2 min) onto the nanopillars. For islets that were unable to be anchored on nanopillars, they were gently spun onto polylysine-coated Fluorodishes and confirmed to be anchored to the plate by gentle rocking. After confirming islets were anchored, 3 ml of PBS at room temperature was added to the Petri dish. Islets ($n = 15$) were interrogated by using AFM (MFP-3D Bio; Asylum Research). We employed a Si with a 5–10-μm colloidal borosilicate glass bead probe (HYDRA2R-100NG-BSG-5 or HYDRA6R-200NG-BSG-10; AppNano). Islets were gently indented in contact mode by the cantilever tip with a trigger force of 500 pN. Deflection data were converted to force by multiplying by the spring constant. To measure Young's modulus, we examined the indentation during extension of the tip into the sample. We fit the function of force *versus* indentation distance by using the Hertz model, using code in the Asylum Research software. We used a Poisson's value of 0.5 for the islets and otherwise default parameters. Stiffness data were imported into R for statistical analysis. Permutation testing was used for statistical comparisons (54).

Hydrogels

Growth factor–reduced Matrigel matrix basal membrane (Corning; Bedford, MA) was diluted to a concentration of 7.5 mg/ml using MilliQ water (H_2O^{∞}, filtered to a resistance of 18.2 MΩ) with 100-kDa sodium hyaluronate (Lifecore Biomedical, Chaska, MN) to achieve final HA weight of 25, 12.5, and 0% (compared with total polymer) while maintaining the equivalent total volumes for each condition. All solutions were kept on ice throughout the preparation. Dynamic oscillatory rheological measurements were conducted with an ARG2 rheometer (TA Instruments, New Castle, DE) with a 20-mm diameter 1° cone angle geometry at a stage temperature of 37 °C. Upon the gel reaching thermal equilibrium, 3-min time sweeps at 10 Hz and 5% strain were conducted on 40-μl samples. Reported data are the result of the average storage modulus (G') from three time sweeps, reported as Young's modulus using the equation of E (Young's modulus) = $2G'(1 + \nu)$, assuming a Poisson's ratio of $\nu = 0.5$ for hydrogels.

Cross-linked hydrogels were formulated using the commercially available thiolated collagen Gelin-S and PEGDA crosslinker Extralink (ESI BIO, Alameda, CA). Gelin-S was reconstituted, and Extralink were reconstituted to 2× and 1× according to manufacturer's specifications, respectively. Gelin-S solutions were mixed with 100-kDa sodium hyaluronate in H_2O^{∞} to form ratios of 25, 12.5, and 0% (sodium hyaluronate:Gelin-S by weight) ensuring same total volume for each formulation. Extralink was added to the solutions following manufacturer recommendations, and 10 μl of hydrogel solution was cast onto fluorodish sample chambers and allowed to cure. PBS buffer was added to the hydrogels to ensure fully hydrated hydrogels prior to AFM measurements. Measurements were conducted as previously described for the pancreatic islets.

Statistics

All other data are expressed as means ± S.E. of n independent measurements. The comparison between two groups was performed with unpaired t tests. A p value < 0.05 was considered statistically significant. Data analysis was performed with the use of GraphPad Prism 5.0 software.

Author contributions—N. N., P. L. B., and M. J. B. conceptualization; N. N., J. P. A., T. N. W., and S. C. H. data curation; N. N., Y. C., J. P. A., T. N. W., S. C. H., P. L. B., and M. J. B. supervision; N. N., P. L. B., and M. J. B. funding acquisition; N. N., A. d. l. Z., G. K., P. Y. J., K. H. H., M. J. K., K. Y., W. Z., G. N., J. P. A., and M. J. B. investigation; N. N., G. K., K. H. H., M. J. K., K. Y., J. P. A., P. L. B., and M. J. B. visualization; N. N., G. K., Y. C., J. P. A., and P. L. B. methodology; N. N., P. L. B., and M. J. B. writing-original draft; N. N., P. L. B., and M. J. B. project administration; N. N., G. K., Y. C., J. P. A., T. N. W., S. C. H., P. L. B., and M. J. B. writing-review and editing; G. K. and K. Y. validation.

References

1. Nyitray, C. E., Chavez, M. G., and Desai, T. A. (2014) Compliant 3D microenvironment improves β-cell cluster insulin expression through mechanosensing and β-catenin signaling. *Tissue Eng. Part A* **20,** 1888–1895 CrossRef Medline

2. Jiang, D., Liang, J., and Noble, P. W. (2011) Hyaluronan as an immune regulator in human diseases. *Physiol. Rev.* **91,** 221–264 CrossRef Medline
3. Laurent, T. C., Laurent, U. B., and Fraser, J. R. (1996) The structure and function of hyaluronan: an overview. *Immunol. Cell Biol.* **74,** A1-A7 CrossRef Medline
4. Vigetti, D., Karousou, E., Viola, M., Deleonibus, S., De Luca, G., and Passi, A. (2014) Hyaluronan: biosynthesis and signaling. *Biochim. Biophys. Acta* **1840,** 2452–2459 CrossRef Medline
5. Fraser, J. R., Laurent, T. C., and Laurent, U. B. (1997) Hyaluronan: its nature, distribution, functions and turnover. *J. Intern. Med.* **242,** 27–33 CrossRef Medline
6. Fraser, J. R., Laurent, T. C., Pertoft, H., and Baxter, E. (1981) Plasma clearance, tissue distribution and metabolism of hyaluronic acid injected intravenously in the rabbit. *Biochem. J.* **200,** 415–424 CrossRef Medline
7. Nieuwdorp, M., Meuwese, M. C., Vink, H., Hoekstra, J. B., Kastelein, J. J., and Stroes, E. S. (2005) The endothelial glycocalyx: a potential barrier between health and vascular disease. *Curr. Opin. Lipidol.* **16,** 507–511 CrossRef Medline
8. Mambetsariev, N., Mirzapoiazova, T., Mambetsariev, B., Sammani, S., Lennon, F. E., Garcia, J. G., and Singleton, P. A. (2010) Hyaluronic acid binding protein 2 is a novel regulator of vascular integrity. *Arterioscler. Thromb. Vasc. Biol.* **30,** 483–490 CrossRef Medline
9. Singleton, P. A., Mirzapoiazova, T., Guo, Y., Sammani, S., Mambetsariev, N., Lennon, F. E., Moreno-Vinasco, L., and Garcia, J. G. (2010) High-molecular-weight hyaluronan is a novel inhibitor of pulmonary vascular leakiness. *Am. J. Physiol. Lung Cell Mol. Physiol.* **299,** L639–L651 CrossRef Medline
10. Khan, A. I., Kerfoot, S. M., Heit, B., Liu, L., Andonegui, G., Ruffell, B., Johnson, P., and Kubes, P. (2004) Role of CD44 and hyaluronan in neutrophil recruitment. *J. Immunol.* **173,** 7594–7601 CrossRef Medline
11. Nagy, N., Freudenberger, T., Melchior-Becker, A., Röck, K., Ter Braak, M., Jastrow, H., Kinzig, M., Lucke, S., Suvorava, T., Kojda, G., Weber, A. A., Sörgel, F., Levkau, B., Ergün, S., and Fischer, J. W. (2010) Inhibition of hyaluronan synthesis accelerates murine atherosclerosis: novel insights into the role of hyaluronan synthesis. *Circulation* **122,** 2313–2322 CrossRef Medline
12. Kang, L., Lantier, L., Kennedy, A., Bonner, J. S., Mayes, W. H., Bracy, D. P., Bookbinder, L. H., Hasty, A. H., Thompson, C. B., and Wasserman, D. H. (2013) Hyaluronan accumulates with high-fat feeding and contributes to insulin resistance. *Diabetes* **62,** 1888–1896 CrossRef Medline
13. Valva, P., Casciato, P., Diaz Carrasco, J. M., Gadano, A., Galdame, O., Galoppo, M. C., Mullen, E., De Matteo, E., and Preciado, M. V. (2011) The role of serum biomarkers in predicting fibrosis progression in pediatric and adult hepatitis C virus chronic infection. *PLoS One* **6,** e23218 CrossRef Medline
14. Yoshioka, Y., Kozawa, E., Urakawa, H., Arai, E., Futamura, N., Zhuo, L., Kimata, K., Ishiguro, N., and Nishida, Y. (2013) Suppression of hyaluronan synthesis alleviates inflammatory responses in murine arthritis and in human rheumatoid synovial fibroblasts. *Arthritis Rheum.* **65,** 1160–1170 CrossRef Medline
15. Back, S. A., Tuohy, T. M., Chen, H., Wallingford, N., Craig, A., Struve, J., Luo, N. L., Banine, F., Liu, Y., Chang, A., Trapp, B. D., Bebo, B. F., Jr, Rao, M. S., and Sherman, L. S. (2005) Hyaluronan accumulates in demyelinated lesions and inhibits oligodendrocyte progenitor maturation. *Nat. Med.* **11,** 966–972 CrossRef Medline
16. Bogdani, M., Johnson, P. Y., Potter-Perigo, S., Nagy, N., Day, A. J., Bollyky, P. L., and Wight, T. N. (2014) Hyaluronan and hyaluronan-binding proteins accumulate in both human type 1 diabetic islets and lymphoid tissues and associate with inflammatory cells in insulitis. *Diabetes* **63,** 2727–2743 CrossRef Medline
17. Ziegler, A. G., and Nepom, G. T. (2010) Prediction and pathogenesis in type 1 diabetes. *Immunity* **32,** 468–478 CrossRef Medline
18. Bollyky, P. L., Bogdani, M., Bollyky, J. B., Hull, R. L., and Wight, T. N. (2012) The role of hyaluronan and the extracellular matrix in islet inflammation and immune regulation. *Curr. Diabetes Reports* **12,** 471–480 CrossRef
19. Nagy, N., Kaber, G., Johnson, P. Y., Gebe, J. A., Preisinger, A., Falk, B. A., Sunkari, V. G., Gooden, M. D., Vernon, R. B., Bogdani, M., Kuipers, H. F., Day, A. J., Campbell, D. J., Wight, T. N., and Bollyky, P. L. (2015) Inhibition of hyaluronan synthesis restores immune tolerance during autoimmune insulitis. *J. Clin. Invest.* **125,** 3928–3940 CrossRef Medline
20. Morgan, J. T., Raghunathan, V. K., Thomasy, S. M., Murphy, C. J., and Russell, P. (2014) Robust and artifact-free mounting of tissue samples for atomic force microscopy. *BioTechniques* **56,** 40–42 Medline
21. Chaurasia, S. S., Champakalakshmi, R., Li, A., Poh, R., Tan, X. W., Lakshminarayanan, R., Lim, C. T., Tan, D. T., and Mehta, J. S. (2012) Effect of fibrin glue on the biomechanical properties of human Descemet's membrane. *PLoS One* **7,** e37456 CrossRef Medline
22. Kultti, A., Pasonen-Seppänen, S., Jauhiainen, M., Rilla, K. J., Kärnä, R., Pyöriä, E., Tammi, R. H., and Tammi, M. I. (2009) 4-Methylumbelliferone inhibits hyaluronan synthesis by depletion of cellular UDP-glucuronic acid and downregulation of hyaluronan synthase 2 and 3. *Exp. Cell Res.* **315,** 1914–1923 CrossRef Medline
23. Nagy, N., Kuipers, H. F., Frymoyer, A. R., Ishak, H. D., Bollyky, J. B., Wight, T. N., and Bollyky, P. L. (2015) 4-Methylumbelliferone treatment and hyaluronan inhibition as a therapeutic strategy in inflammation, autoimmunity, and cancer. *Front. Immunol.* **6,** 123 Medline
24. Hull, R. L., Bogdani, M., Nagy, N., Johnson, P. Y., and Wight, T. N. (2015) Hyaluronan: a mediator of islet dysfunction and destruction in diabetes? *J. Histochem. Cytochem.* **63,** 592–603 CrossRef Medline
25. Xie, C., Hanson, L., Xie, W., Lin, Z., Cui, B., and Cui, Y. (2010) Noninvasive neuron pinning with nanopillar arrays. *Nano Lett.* **10,** 4020–4024 CrossRef Medline
26. Hanson, L., Zhao, W., Lou, H. Y., Lin, Z. C., Lee, S. W., Chowdary, P., Cui, Y., and Cui, B. (2015) Vertical nanopillars for in situ probing of nuclear mechanics in adherent cells. *Nat. Nanotechnol.* **10,** 554–562 CrossRef Medline
27. Serban, M. A., Scott, A., and Prestwich, G. D. (2008) Use of hyaluronan-derived hydrogels for three-dimensional cell culture and tumor xenografts. *Curr. Protoc. Cell Biol.* Chapter 10, Unit 10.14 Medline
28. Assavag-Asherie, N., Sever, D., Bogdani, M., Johnson, P., Weiss, T., Ginzberg, A., Perles, S., Weiss, L., Sebban, L. E., Turley, E. A., Okon, E., Raz, I., and Naor, D. (2015) Can CD44 be a mediator of cell destruction?: The challenge of type 1 diabetes. *PLoS One* **1,** e0143589 Medline
29. Harrington, S., Williams, J., Rawal, S., Ramachandran, K., and Stehno-Bittel, L. (2017) Hyaluronic acid/collagen hydrogel as an alternative to alginate for long-term immunoprotected islet transplantation. *Tissue Eng. Part A* **23,** 1088–1099 CrossRef Medline
30. Cavallari, G., Olivi, E., Bianchi, F., Neri, F., Foroni, L., Valente, S., La Manna, G., Nardo, B., Stefoni, S., and Ventura, C. (2012) Mesenchymal stem cells and islet cotransplantation in diabetic rats: improved islet graft revascularization and function by human adipose tissue-derived stem cells preconditioned with natural molecules. *Cell Transplant.* **21,** 2771–2781 CrossRef Medline
31. Li, Y., Nagira, T., and Tsuchiya, T. (2006) The effect of hyaluronic acid on insulin secretion in HIT-T15 cells through the enhancement of gap-junctional intercellular communications. *Biomaterials* **27,** 1437–1443 CrossRef Medline
32. Velten, F., Laue, C., and Schrezenmeir, J. (1999) The effect of alginate and hyaluronate on the viability and function of immunoisolated neonatal rat islets. *Biomaterials* **20,** 2161–2167 CrossRef Medline
33. Kato, Y., Mukudai, Y., Okimura, A., Shimazu, A., and Nakamura, S. (1995) Effects of hyaluronic acid on the release of cartilage matrix proteoglycan and fibronectin from the cell matrix layer of chondrocyte cultures: interactions between hyaluronic acid and chondroitin sulfate glycosaminoglycan. *J. Rheumatol. Suppl.* **43,** 158–159 Medline
34. Responte, D. J., Natoli, R. M., and Athanasiou, K. A. (2012) Identification of potential biophysical and molecular signalling mechanisms underlying hyaluronic acid enhancement of cartilage formation. *J. R. Soc. Interface* **9,** 3564–3573 CrossRef Medline
35. Rehfeldt, F., Brown, A. E., Raab, M., Cai, S., Zajac, A. L., Zemel, A., and Discher, D. E. (2012) Hyaluronic acid matrices show matrix stiffness in 2D and 3D dictates cytoskeletal order and myosin-II phosphorylation within stem cells. *Integr. Biol.* (*Camb.*) **4,** 422–430 Medline
36. Screen, H. R., Chhaya, V. H., Greenwald, S. E., Bader, D. L., Lee, D. A., and Shelton, J. C. (2006) The influence of swelling and matrix degrada tion on

the microstructural integrity of tendon. *Acta Biomater.* **2,** 505–513 CrossRef Medline
37. Engler, A. J., Sen, S., Sweeney, H. L., and Discher, D. E. (2006) Matrix elasticity directs stem cell lineage specification. *Cell* **126,** 677–689 CrossRef Medline
38. Gilbert, P. M., Havenstrite, K. L., Magnusson, K. E., Sacco, A., Leonardi, N. A., Kraft, P., Nguyen, N. K., Thrun, S., Lutolf, M. P., and Blau, H. M. (2010) Substrate elasticity regulates skeletal muscle stem cell self-renewal in culture. *Science* **329,** 1078–1081 CrossRef Medline
39. Chaudhuri, O., Koshy, S. T., Branco da Cunha, C., Shin, J. W., Verbeke, C. S., Allison, K. H., and Mooney, D. J. (2014) Extracellular matrix stiffness and composition jointly regulate the induction of malignant phenotypes in mammary epithelium. *Nat. Mater.* **13,** 970–978 CrossRef Medline
40. Kumar, S., and Weaver, V. M. (2009) Mechanics, malignancy, and metastasis: the force journey of a tumor cell. *Cancer Metastasis Rev.* **28,** 113–127 CrossRef Medline
41. Kuipers, H. F., Rieck, M., Gurevich, I., Nagy, N., Butte, M. J., Negrin, R. S., Wight, T. N., Steinman, L., and Bollyky, P. L. (2016) Hyaluronan synthesis is necessary for autoreactive T-cell trafficking, activation, and Th1 polarization. *Proc. Natl. Acad. Sci. U.S.A.* **113,** 1339–1344 CrossRef Medline
42. Wolf, K., and Friedl, P. (2011) Extracellular matrix determinants of proteolytic and non-proteolytic cell migration. *Trends Cell Biol.* **21,** 736–744 CrossRef Medline
43. Mueller, A. M., Yoon, B. H., and Sadiq, S. A. (2014) Inhibition of hyaluronan synthesis protects against central nervous system (CNS) autoimmunity and increases CXCL12 expression in the inflamed CNS. *J. Biol. Chem.* **289,** 22888–22899 CrossRef Medline
44. Day, A. J., and Prestwich, G. D. (2002) Hyaluronan-binding proteins: tying up the giant. *J. Biol. Chem.* **277,** 4585–4588 CrossRef Medline
45. Day, A. J., and de la Motte, C. A. (2005) Hyaluronan cross-linking: a protective mechanism in inflammation? *Trends Immunol* **26,** 637–643 CrossRef Medline
46. Ruppert, S. M., Hawn, T. R., Arrigoni, A., Wight, T. N., and Bollyky, P. L. (2014) Tissue integrity signals communicated by high-molecular weight hyaluronan and the resolution of inflammation. *Immunol. Res.* **58,** 186–192 CrossRef Medline
47. Carrero, J. A., Calderon, B., Towfic, F., Artyomov, M. N., and Unanue, E. R. (2013) Defining the transcriptional and cellular landscape of type 1 diabetes in the NOD mouse. *PLoS One* **8,** e59701 CrossRef Medline
48. Irving-Rodgers, H. F., Ziolkowski, A. F., Parish, C. R., Sado, Y., Ninomiya, Y., Simeonovic, C. J., and Rodgers, R. J. (2008) Molecular composition of the peri-islet basement membrane in NOD mice: a barrier against destructive insulitis. *Diabetologia* **51,** 1680–1688 CrossRef Medline
49. Lieleg, O., Baumgärtel, R. M., and Bausch, A. R. (2009) Selective filtering of particles by the extracellular matrix: an electrostatic bandpass. *Biophys. J.* **97,** 1569–1577 CrossRef Medline
50. Lieleg, O., and Ribbeck, K. (2011) Biological hydrogels as selective diffusion barriers. *Trends Cell Biol.* **21,** 543–551 CrossRef Medline
51. Swartz, M. A., and Fleury, M. E. (2007) Interstitial flow and its effects in soft tissues. *Annu. Rev. Biomed. Eng.* **9,** 229–256 CrossRef Medline
52. Bollyky, P. L., Bice, J. B., Sweet, I. R., Falk, B. A., Gebe, J. A., Clark, A. E., Gersuk, V. H., Aderem, A., Hawn, T. R., and Nepom, G. T. (2009) The toll-like receptor signaling molecule Myd88 contributes to pancreatic beta-cell homeostasis in response to injury. *PLoS One* **4,** e5063 CrossRef Medline
53. Evanko, S. P., Potter-Perigo, S., Bollyky, P. L., Nepom, G. T., and Wight, T. N. (2012) Hyaluronan and versican in the control of human T-lymphocyte adhesion and migration. *Matrix Biol.* **31,** 90–100 CrossRef Medline
54. Hesterberg, T. (2015) Resample: resampling functions. R package version 0.4